Pergamon

Int. J. Solids Structures Vol. 35, Nos 28–29, pp. 3695–3715, 1998

0020-7683/98 $19.00 + .00

PII: S0020-7683(97)00236-9

ANTIPLANE SHEAR CRACK GROWTH UNDER QUASISTATIC LOADING IN A DAMAGING MATERIAL

B. YANG and K. RAVI-CHANDAR*
Department of Mechanical Engineering, University of Houston, Houston, TX 77204-4792, U.S.A.

(*Received* 3 *December* 1996; *in revised form* 24 *June* 1997)

Abstract—Antiplane shear crack growth is examined numerically in a precracked rectangular specimen subjected to quasi-static antisymmetric loading, by cohesive layer modeling. Material in the cohesive layer ahead of the crack tip is modeled to be linear elastic-softening with a damaging locus while bulk material of the specimen is assumed to be linear elastic. The evolution of physical and fictitious crack tips is obtained from solutions to the boundary value problem formulated. Critical values of the J-integral and crack opening displacement (COD) for onset of either stable or unstable crack growth are examined, and shown to be dependent upon initial crack length, loading distribution as well as material properties. It is also shown that a unique relationship between a critical value of J integral and a critical COD cannot be obtained in general. The iterative method of Successive-Over-Relaxation (SOR) is applied in the present work. © 1998 Elsevier Science Ltd. All rights reserved.

1. INTRODUCTION

In the conventional fracture mechanics approach, based on the ideas of Griffith, the details of the dissipative processes that occur in the fracture process leading to crack growth are typically ignored and only the total energy necessary for the crack to extend is considered. However, in a number of different types of nominally brittle materials, such as concrete, ceramics, polymers and composites, fracture occurs typically through the development of a large fracture process zone ahead of the crack line and the partially damaged material in this process zone is softening relative to the bulk material; ignoring this process zone results in an incorrect characterization of crack initiation, growth and stability. Recognizing this, Dugdale (1960) and Barenblatt (1962) originally considered a simple line process zone model to incorporate the effect of crack tip plasticity or cohesive atomic forces. Since this early development, the idea of a fracture process zone or a *cohesive zone*, has been applied in investigating crack growth in the kind of materials described above. This literature is vast and it is not our intent to review these in detail; rather, we shall summarize the different approaches that have been used in the analysis of the cohesive crack problem.

In these cohesive zone models, since the inelastic (damage softening) material is confined to the process zone and since deformation in the direction perpendicular to the crack line within the cohesive zone is considered to be uniform, a simple force-displacement relationship, $\sigma = f(w)$, is used to characterize the mechanical behavior within the cohesive zone; Smith (1974) investigated possible shapes for the softening part of this function. With the prescription of this constitutive law for the cohesive zone material, the global behavior of a cracked solid as well as the evolution of the cohesive zone itself can be investigated as a mixed boundary value problem of the surrounding continuum; the only difference from a standard crack problem is that at the boundary of the cohesive zone the tractions and displacements must obey the constitutive law prescribed for the cohesive zone material. Note that the length of the cohesive zone, α, is not known *a priori* and has to be determined as part of the solution. A number of different approaches have been used to analyze crack problems within the context of the cohesive zone model; they fall broadly into four categories. The classical approach is to use the idea of Dugdale and Barenblatt

* Author to whom correspondence should be addressed.

and impose the condition that the stresses near the crack tip must be nonsingular and hence that the stress intensity factor resulting from externally applied forces and the cohesive forces must cancel each other out; this requirement is sufficient to determine the length of the cohesive zone. The works of Knauss (1974), Schapery (1975) and many others that examined the problem of crack growth in viscoelastic materials fall into this category. The second approach is to consider that the cohesive zone does not completely cancel out the singularity, but only shields the crack tip partially; this implies that a critical stress intensity factor at crack initiation is still necessary as an additional material parameter in order to determine the length of the cohesive zone. Cox and Marshall (1994) refer to this as a bridged crack model as distinguished from a cohesive zone that has no singularity; the bridged crack models are then characterized in terms of a stress intensity factor based fracture resistance curve. The third approach introduced by Hillerborg *et al.* (1976) is called the fictitious crack model; in this model, the cohesive zone tip position is fixed arbitrarily and then the corresponding applied loading and crack opening profile are computed numerically; Carpenteri (1994) describes this model and its numerical implementation in detail for a three-point bend specimen. A large number of computations are necessary in order to determine the load to load-point displacement variation in this approach, but the idea of a stress intensity factor is not really necessary in this approach. One drawback of this approach seems to be in the generalization to arbitrarily distributed loading; the calculation of the influence functions and the relationship between the far field loading and the cohesive zone displacements appears to be difficult to handle in general. The last approach is to consider a thin layer ahead of the crack tip to be made up completely of the cohesive zone material and to solve the resulting mixed boundary value problem completely including the nonlinear boundary condition representing the cohesive layer material. Andersson and Bergkvist (1970) used this approach and formulated the mixed boundary value problem in terms of an integral equation which was solved numerically; in this problem, the cohesive zone initiates and grows with the prescription of the boundary loading, without the use of local failure criteria other than the cohesive zone material properties. Knauss (1974) and Ungsuwarungsri and Knauss (1987) have also used the layer approach to examine crack extension in viscoelastic materials. This last approach of using a cohesive layer model is the most general and efficient one in terms of applications as has been demonstrated more recently by Xu and Needleman (1994) and Ortiz (1996) who considered the use of the cohesive zone models in finite element simulations of crack growth and fragmentation problems. In the present paper, we use a similar cohesive layer description of fracture to examine quasi-static crack growth behavior.

In order to obtain the global cracking behavior and the local process zone evolution, in the present work we apply a model similar to that used by Andersson and Bergkvist (1970), and Ungsuwarungsri and Knauss (1987). A thin layer which is characterized by an elastic-softening law is inserted between two finite rectangular linear elastic plates. When generalizing the cohesive zone model to arbitrary loading histories and crack paths, one has to provide the possibility for unloading of the specimen without recovery of the cohesive zone materials. The incorporation of a damage parameter that tracks the current state of each point on the cohesive zone allows for the possibility of partial damage, unloading and reloading effects. Also, a pre-existing crack is generated simply by the removal of part of the cohesive layer, while a pre-existing crack tip process zone is described by imposing initial damage to the layer material in the process zone or damaged zone. The details of the cohesive layer model employed in this work are described in Section 2.2. Only two-dimensional anti-plane shear cracking under quasi-static loading is considered in this paper, but extension to the in-plane symmetric loading is straightforward; the case of dynamic loading has been considered elsewhere (Yang and Ravi-Chandar, 1996). The geometry and initial and loading conditions are such that it is ensured that the crack extends along the middle line of the cohesive layer; note that this dictates the crack to lie along the line of symmetry. The corresponding boundary value problem is formulated for quasi-static loading in Section 2.3. The reformulation of the problem in a finite difference form and the solution procedure using the iterative method of Successive-Over-Relaxation (SOR) are described in Section 3. Crack growth occurs in this simulation naturally by continuous separation of the layer

material; the results of a number of simulations exploring crack initiation, growth and stability are discussed in Section 4. From the numerical solution to the cohesive crack problem, the evolution of the leading and trailing points of the process zone which are the physical and fictitious crack tips respectively, and the evolution of the cohesive zone size are obtained. The global cracking behavior under two kinds of loading distribution are investigated in Sections 4.1 and 4.2; cracking of the specimen is unstable no matter how long the initial crack length is when loading is applied to the boundaries parallel to the crack line, but there exists a mode transition from stable crack growth to unstable crack growth with variation of the crack length when loading is applied to the boundary perpendicular to the crack line, with fixed material properties. These simulations are used in Section 4.3 to examine the crack tip characterizing parameters such as a critical crack opening displacement (COD) or a J-integral. The commonly used concept of fracture-energy-determinant cracking is examined in Section 4.4 by changing the profile of the damage locus in the cohesive layer material, but keeping the energy release rate constant. It is demonstrated that different cohesive zone constitutive laws might still provide the same global structural response suggesting that local measurements are essential in order to establish the constitutive properties of the cohesive layer.

2. THE COHESIVE CRACK MODEL OF AN ANTI-PLANE SHEAR CRACK

2.1. *Configuration*

Consider a crack in a rectangular specimen of dimensions $a \times 2b$ subjected to antiplane loading as shown in Fig. 1a. A thin layer of uniform thickness $2d$ is imposed on the line ahead of the crack tip. The layer material is modeled in the sequel to be of the elastic-softening type while the bulk material is assumed to be linearly elastic. In nominally brittle materials, this layer can be considered to be the damage zone developed by the enhanced stress field near the crack tip, through microcrack nucleation, growth and coalescence. It can also model a craze zone in some polymers (Ungsuwarungsri and Knauss, 1987, Kendall *et al.*, 1991), a wake zone in some ceramics (Bennison and Lawn, 1989, Hay, 1995), and a fiber-bridging zone in some composites (Marshall *et al.*, 1985, Bosco *et al.*, 1995). No matter which mechanism is relevant to the particular material, a softening constitutive law seems appropriate to characterize the materials in the zones. For the present purposes, we shall simply assume an idealized constitutive law of the layer material below and examine its consequences on crack growth. The initial and boundary conditions are such that it is ensured that the crack proceeds along the middle line of the layer, with macro-branching

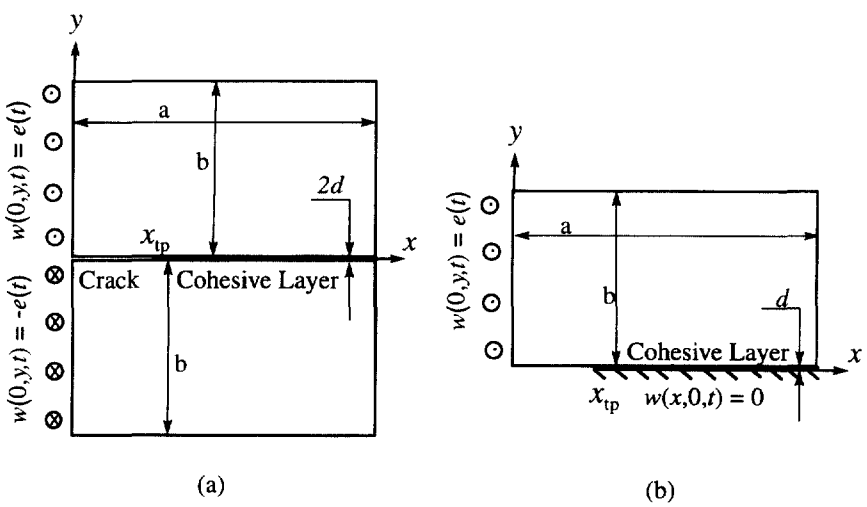

Fig. 1. (a) Geometry of the crack in a finite rectangular specimen under anti-plane shear loading with a cohesive layer material ahead of the crack tip, along the line $y = 0$; (b) geometry of the equivalent problem with zero displacement along the line $y = 0$.

assumed to be absent. This is equivalent to assuming that a thin adhesive layer exists, joining two elastic plates; thus the present model should describe adhesive joints as well.

2.2. *Behavior of the layer material*

It is common practice to describe the cohesive material model as a force-displacement jump relation across the cohesive layer. We prefer to describe the layer behavior in terms of a cohesive stress-strain law together with a layer thickness assuming uniform deformation in the layer thickness direction within the layer; the cohesive layer thickness may not remain constant in experiments, but depends on the constraint applied on the geometry of the specimen; with a view towards developing an evolution equation for the cohesive layer thickness that would then dictate the total energy dissipation in the layer, it is advantageous to describe the cohesive zone through a stress-strain law rather than a force-displacement jump relation. However, in the simulations presented in this paper, the two descriptions are equivalent.

The layer material behavior is modeled to be linearly elastic with a variable shear modulus, k, which softens with damage, as shown schematically in Fig. 2. The shear modulus, k, is determined by the maximum strain, γ_d, that the material has ever experienced, indicating the irrecoverable damage state. γ_d is used here as the measure of current damage and will be called the *damaging strain*. If the layer is strained above γ_d, further damage occurs and k softens further; otherwise, k is constant. This material behavior is expressed by

$$\tau_{layer} = k\gamma_{layer} \quad \text{for } 0 \leqslant \gamma_{layer} \leqslant \gamma_d, \tag{1}$$

where τ_{layer} and γ_{layer} are the shear stress and strain in the layer material respectively, and

$$k = \bar{k}(\gamma_d), \tag{2}$$

where $\bar{k}$ is a decreasing function of γ_d, indicating the softening behavior of the material. Corresponding to each γ_d, there exists a damaging stress, τ_d, and a *damage locus* derived from eqns (1) and (2),

$$\tau_d = \bar{\tau}_d(\gamma_d). \tag{3}$$

In general, we have two critical states on this locus. One is at $\gamma_d = \gamma_y$, the threshold strain for the start of damage in the material; below this strain level, k is a constant equal to its

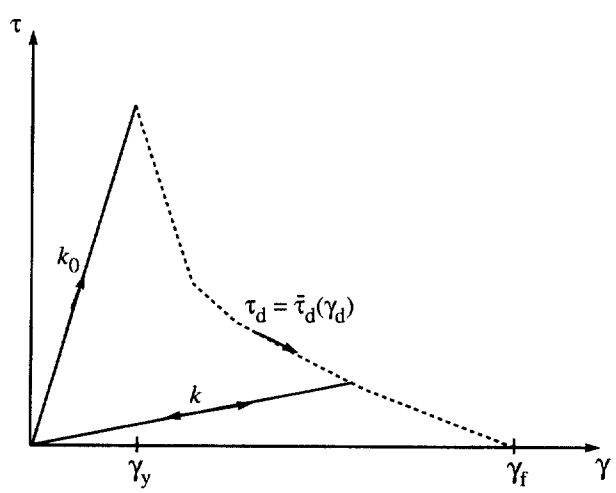

Fig. 2. Constitutive behavior of the cohesive layer material; the dashed line indicates arbitrary damage locus of non-positive slope.

maximum value indicated by k_0. The other is at $\gamma_d = \gamma_f$, the separation strain, indicating the complete failure of the material, beyond which k is equal to zero. These two critical states will be used to define the physical and fictitious crack tips and consequently the fracture process zone between them.

Under monotonic loading, the model material behaves linearly at its initial elastic modulus until it reaches the damage locus, and then softens along the locus until the complete separation of the material occurs; this is the behavior considered in cohesive layer modeling in most of the previous work cited. In the present constitutive model for the layer, unloading and reloading behavior of the material are modeled as well, as shown schematically in Fig. 2; this enables a simulation of the crack growth under arbitrary loading conditions. In addition, the present model also allows for a pre-damaged process zone to exist; this is prescribed simply by defining that the initial modulus varies in the pre-existing process zone from k_0 to zero. Thus, the cohesive zone material could occupy all the points below the damage locus in Fig. 2. In this constitutive description of the layer material, it is assumed implicitly that residual strain due to the damage is zero; however, this can be adjusted easily to take into account non-trivial residual strains. This cohesive zone model, albeit in a slightly different form, was used by Yang and Ravi-Chandar (1996) to study the role of the fracture process zone on dynamic crack growth. The constitutive behavior described above for the cohesive layer is based on phenomenological considerations of the breakdown of the crack tip material; accurate description of the material behavior can be obtained either through careful experiments or through a micromechanical model of the process of breakdown of the crack tip material. In either case, one needs to link the microscale (crack tip process zone scale) parameters to the macroscale (structure size) parameters; we will explore this aspect later in Sections 4.3 and 4.4.

2.3. *Governing equations*

The quasi-static two-dimensional anti-plane deformation of the homogeneous, isotropic, linear elastic specimen excluding the layer material is determined by the out-of-plane displacement, $w(x,y,t)$, which satisfies Laplace's equation

$$\frac{\partial^2 w}{\partial x^2} + \frac{\partial^2 w}{\partial y^2} = 0. \tag{4}$$

Note that time is used only to indicate history of w, and is not a natural time scale. In terms of the non-zero displacement w, the non-zero elastic stress components are expressed as

$$\sigma_{zx} = \mu \frac{\partial w}{\partial x}, \sigma_{zy} = \mu \frac{\partial w}{\partial y}, \tag{5}$$

where μ is the shear modulus of the material. The initial damage distribution in the layer is assumed to be given by

$$k(x) = \begin{cases} 0 & 0 \leqslant x < x_{tp} \\ k_{pz}(x) & \text{for } x_{tp} \leqslant x \leqslant x_{lp}, \\ k_0 & x_{lp} < x \leqslant a \end{cases} \tag{6}$$

where x_{lp} is the leading point of the process zone sometimes called the fictitious crack tip and is defined as the first point of the layer of modulus equal to k_0, and x_{tp} is the trailing point of the process zone or the physical crack tip and is defined as the first point of the layer of modulus not equal to zero. k_{pz} is a prescribed monotonic and continuous function of x, defining the state of a pre-existing process zone, with

$$k_{pz}(x_{tp}) = 0 \quad \text{and} \quad k_{pz}(x_{lp}) = k_0. \tag{7}$$

The layer thickness, $2d$, is small compared with the length scale of the specimen, and is neglected in the description of the conditions below. Loading is applied on the left boundary $x = 0$:

$$w(0, y, t) = \begin{cases} e(t) & 0^+ \leqslant y \leqslant b \\ -e(t) & -b \leqslant y \leqslant 0^- \end{cases} \text{for}, \tag{8}$$

where $e(t)$ is a prescribed function for $t \geqslant 0$, with $e(0) = 0$. The top, bottom and right boundaries are traction free, which for a linearly elastic material may be written as

$$\mu \frac{\partial w}{\partial y}(x, b, t) = 0 \quad \text{for } 0 \leqslant x \leqslant a, \tag{9}$$

$$\mu \frac{\partial w}{\partial y}(x, -b, t) = 0 \quad \text{for } 0 \leqslant x \leqslant a, \tag{10}$$

and

$$\mu \frac{\partial w}{\partial x}(a, y, t) = 0 \quad \text{for } -b \leqslant y \leqslant b. \tag{11}$$

One notes the anti-plane symmetry of the displacement field relative to the middle line of the cohesive layer $y = 0$, $w(x,y,t) = -w(x,-y,t)$, under these boundary conditions. Hence the displacement along $y = 0$ is zero. The deformation of the thin layer is assumed to vary uniformly in y-direction. Thus the shear strain in the layer is calculated by

$$\gamma_{layer}(x, t) = (w(x, 0^+, t) - w(x, 0^-, t))/2d = w(x, 0^+, t)/d. \tag{12}$$

The continuity of traction across the two interfaces between the elastic plates and the cohesive layer material requires

$$\left.\begin{aligned} \mu \frac{\partial w}{\partial y}(x, 0^+, t) &= \bar{\tau}_{layer}(k, \gamma_{layer}(x, t)) \\ \mu \frac{\partial w}{\partial y}(x, 0^-, t) &= \bar{\tau}_{layer}(k, \gamma_{layer}(x, t)) \end{aligned}\right\} \quad \text{for } 0 \leqslant x \leqslant a, \tag{13}$$

where $\bar{\tau}_{layer}(k, \gamma_{layer})$ is the function defined by eqn (1), and k is determined by eqn (2). Now the complete anti-plane shear problem is to find the unknown, $w(x,y,t)$ that satisfies eqns (1) (2) (4) and (6) through (13). Note that the evolution of the crack tips, x_{lp} and x_{tp}, in this geometry under this loading condition, has been implied in the solution to the problem formulated above, and is a function of the loading amplitude $e(t)$, and hence a function of time t. Thus the problem of crack extension has been written down completely in the form of a boundary value problem whose solution may be generated numerically. In the next section, we illustrate a finite difference implementation of the solution; one could equally well adapt this problem to a finite element formulation. Also, a corresponding formulation of the cohesive layer problem can easily be written down for the case of a mode I crack problem, with the restriction of crack extension along the line of symmetry.

3. NUMERICAL IMPLEMENTATION

As mentioned above, due to the anti-symmetry of the displacement field $w(x,y,t)$ relative to the crack line, we need consider only the upper half of the geometry as shown in

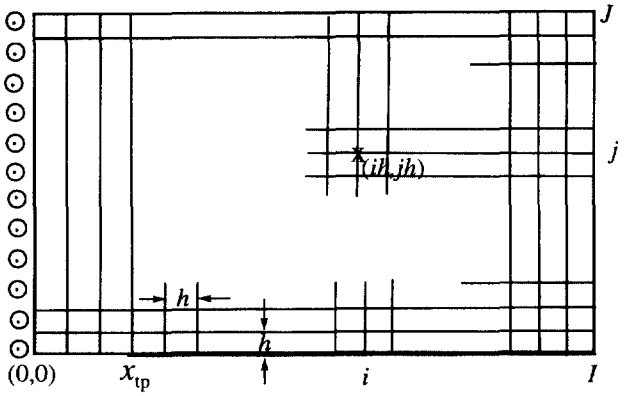

Fig. 3. Discretization of the domain of $a \times b$ under consideration.

Fig. 1b. For a numerical solution of the problem, the region $0 \leqslant x \leqslant a$, $0^{+} \leqslant y \leqslant b$, is discretized into an $(I+1) \times (J+1)$ rectangular grid with a uniform mesh size in both the x and y directions, with $\Delta x = \Delta y = h$, as shown in Fig. 3. The nodes are at

$$(x(i), y(j)) = (ih, jh) \quad i = 0, 1, 2, \ldots, I \quad \text{and} \, j = 0, 1, 2, \ldots, J, \text{respectively.} \tag{14}$$

The displacement $w(x,y,t)$ is denoted by

$$w(x(i), y(j), t_n) = w_{i,j}^{n} \quad \text{for} \begin{matrix} i = 0, 1, 2, \ldots, I \quad \text{and} \, j = 0, 1, 2, \ldots, J \\ n = 0, 1, 2, \ldots \end{matrix}, \tag{15}$$

where n is the current time step, and t_n is the current time. We have, in general, two strategies to solve Laplace's equation numerically. One strategy is to form an algebraic system of equations for the nodes and solve it directly; the other is by an iterative process. As a matter of fact, in our case, the former strategy is not exactly straightforward at all. The history-dependent behavior of the cohesive layer material necessitates the use of the iterative process. We choose in the present work the iterative method of SOR. Laplace's equation is then discretized and arranged into the SOR iterative form:

$$w_{i,j}^{n,m+1} = w_{i,j}^{n,m} + \alpha \left(\frac{w_{i+1,j}^{n,m} + w_{i-1,j}^{n,m+1} + w_{i,j+1}^{n,m+1} + w_{i,j-1}^{n,m} - 4w_{i,j}^{n,m}}{4} \right), \tag{16}$$

for calculation of the internal nodes, in which m is the iterative step, and α is the adjustable relaxation factor. Maximum acceleration is obtained for some optimum value of α, which always lies between 1 and 2 for Laplace's equation. However, it is not obtained in general for the problem of arbitrary geometry. For the rectangular region having constant boundary conditions, the optimum α is given by

$$\alpha_{opt} = \frac{4}{2 + \sqrt{4 - \beta^2}}, \tag{17}$$

with

$$\beta = \cos\frac{\pi}{I} + \cos\frac{\pi}{J}. \tag{18}$$

Such a calculation is applied for α in the present simulations. However, it may not be the optimum α in the present case with a boundary condition of the cohesive layer which is

neither a typical displacement condition nor a typical traction condition. The left boundary condition along $x = 0$ is discretized as

$$w_{0,j}^{n,m+1} = e(t_n) \quad \text{for } j = 0, 1, 2, \ldots, J. \tag{19}$$

The top boundary condition along $y = b$ is discretized as

$$w_{i,J}^{n,m+1} = w_{i,J-1}^{n,m} \quad \text{for } i = 1, 2, \ldots, I. \tag{20}$$

The right boundary condition along $x = a$ is discretized in the form

$$w_{I,j}^{n,m+1} = w_{I-1,j}^{n,m+1} \quad \text{for } j = 1, 2, \ldots, J. \tag{21}$$

Finally we handle the layer boundary nodes below. The interfacial condition is numerically implemented for each node i by a process which is in general iterative; at the layer boundary, the displacement is given by

$$w_{i,0^+}^{n,m+1} = \frac{1}{1 + (h/d)(k_{i,0^+}^{n,m}/\mu)} w_{i,1}^{n,m-1}; \tag{22}$$

if $w_{i,0^+}^{n,m+1}/d \leqslant \gamma_{di,0^+}^{n-1}$, there is no further damage and the calculation is done; otherwise, the new softened shear modulus calculated by

$$k_{i,0^+}^{n,m+1} = \bar{k}(w_{i,0^+}^{n,m+1}/d), \tag{23}$$

where $\bar{k}$ is the function defined in eqn (2). Then the calculation reverts to eqn (22) with $k_{i,0^+}^{n,m+1}$ if the difference of $k_{i,0^+}^{n,m+1}$ from the previous iteration step is still larger than the desired value; otherwise, the iteration is terminated.

The practical computational process is to assign the values to the left boundary nodes by eqn (19), then to calculate the values of the top boundary nodes by eqn (20), then to calculate the values of the internal nodes by eqn (16), then to calculate the values of the right boundary nodes by eqn (21), and finally to handle the layer boundary nodes by eqns (22) and (23). The average of the absolute difference of the displacement of all the nodes in the current iterative step from that in the previous step is used for the judgment of the accuracy of the iterative process. If it is below the desired value, the iterative process is terminated; otherwise, the iteration reverts to eqn (19) and repeats. The SOR iterative finite difference formulation of the anti-plane cohesive crack model of the quasi-static fracture problem was used in a number of simulations of the crack problem described in the next section.

4. SIMULATIONS OF QUASI-STATIC CRACK GROWTH AND DISCUSSION

4.1. *Edge loading*

We begin with a simulation of the quasi-static crack growth in the finite rectangular specimen with $b/a = 0.5$. There are two length scales in this fracture problem: the first length scale is the structural length characterized by the specimen width a, and the second length scale is fracture process characterizing length scale which is idealized as the cohesive layer thickness d and taken to be equal to 0.01 a. For normalization of length quantities we use either d or a, depending on the quantity of interest: specimen geometrical quantities such as the crack length are normalized with the specimen width a, while the crack opening displacement and the fracture process zone size are normalized by the layer thickness d.

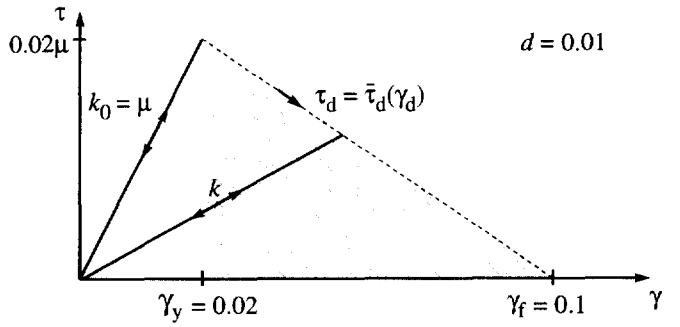

Fig. 4. An idealized constitutive law of the cohesive layer material; the initial stiffness is taken to be identical to that of the bulk material. The dashed straight line of negative slope indicates the damage locus. The shaded area is the energy per unit volume dissipation in the process zone during stable crack growth; the elastic energy is assumed able to be recovered, although this has no consequence on the stability.

For simplicity, we assume the damage locus to be linear, as shown in Fig. 4. The other material properties are taken to be as follows: $k_0 = \mu$, $\gamma_y = 0.02$, and $\gamma_f = 0.1$. The accuracy-governing parameter of the iteration described above is equal to 2E-12. The crack tips are initially at $x_{tc} = 0.1\,a$ and $x_{tv} = 0.11\,a$ respectively, between which k increases linearly from 0 to k_0. The size of the pre-existing process zone is correspondingly equal to the layer thickness d, and is smaller than the one for stable crack growth that will be obtained later. The mesh divisions in the x and y directions, I and J are 300 and 150 respectively, and hence $h = a/300$; convergence studies using different size meshes indicated that this mesh refinement was sufficient to capture the evolution of the cohesive zone (Yang, 1996). Jagota and Bennison (1995) discuss the mesh size dependence of discrete models of fracture; in particular, they point out that finite element schemes are better suited for discretized fracture models than spring-network models. In the present model, however, there exists an intrinsic length scale—*the equilibrium cohesive zone length*; if the mesh discretization is sufficient to resolve this length scale, the numerical results should become mesh insensitive. The imposed displacement, $e(t)$, on the left boundary of the specimen is quasi-static, as shown in Fig. 5. The results of the simulation are described below:

- While the calculation is conducted progressively in time, the positions of the leading and trailing points of the process zone, x_{lp} and x_{tp}, are tracked in terms of the imposed displacement e, and accordingly the process zone size $(x_{lp} - x_{tp})$, is determined in terms of e, as shown in Figs 6a and 6b respectively.
- At each time step, the force per unit length in the z direction, f, is obtained through integration of the traction along the upper half of the left loading boundary, and is plotted

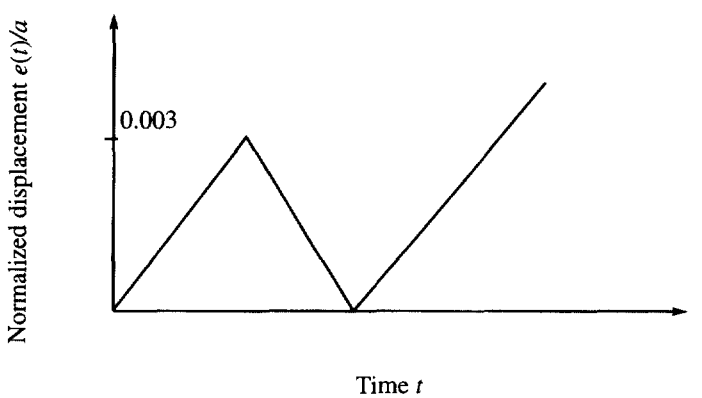

Fig. 5. Time variation of the imposed displacement boundary condition at $x = 0$.

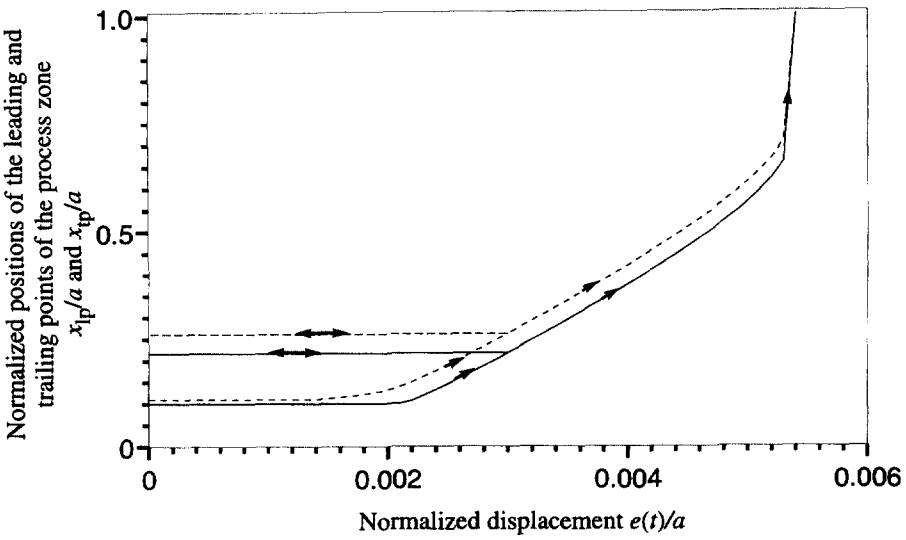

(a)

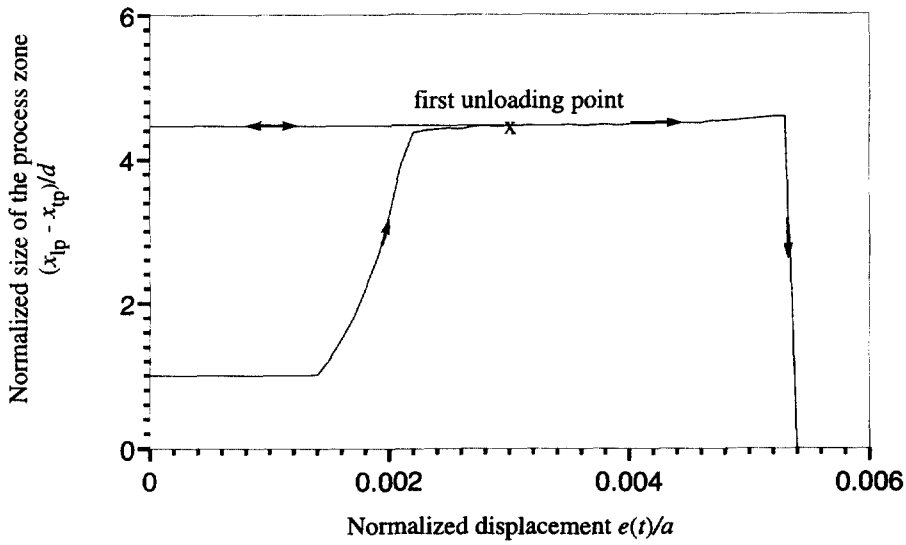

(b)

Fig. 6. Response of the process zone under the loading shown in Fig. 5: (a) evolution of the leading (dashed) and trailing (solid) points of the process zone; (b) evolution of the process zone size.

against e in Fig. 7; this corresponds to the load vs the load-point displacement variation that are typically measured in experiments.

- Since the initial process zone size length, set equal to the layer thickness d, is relatively small, the fictitious crack tip, x_{lp}, develops first, followed later by the growth of the physical crack tip, x_{tp}, with a fully developed process zone of length of approximately 4.5 d as shown in Fig. 6b—*this is the equilibrium cohesive zone length* for this particular loading configuration.
- During the unloading period, the crack remains stationary with the damaged cohesive layer being irrecoverable; the unloading load-displacement curve in Fig. 7 shows the reduced stiffness caused by the crack growth.
- When reloaded, the load-displacement relation is again along the unloading path and the crack starts to move under a displacement beyond the peak of the first cycle.
- When the amplitude of the displacement-controlled reloading approaches a critical value, the crack growth, still with a large unbroken ligament, becomes unstable. The crack

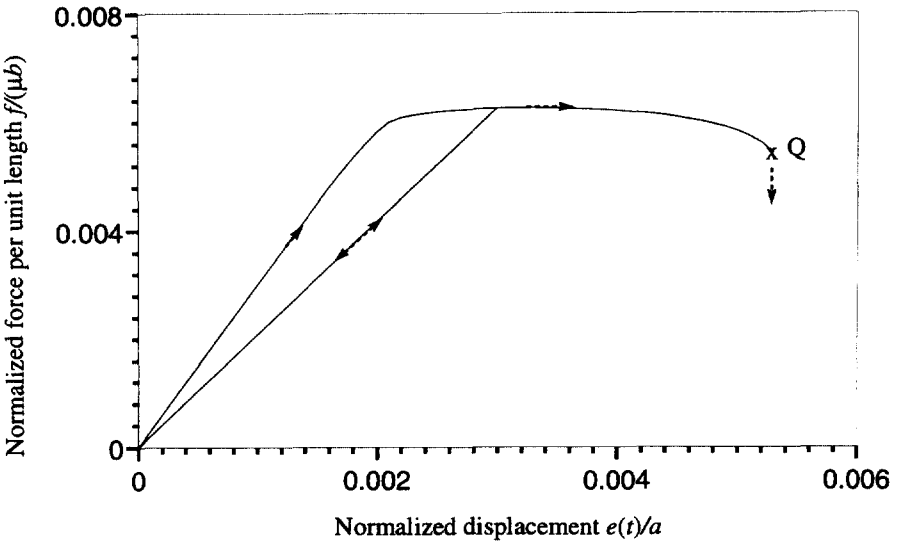

Fig. 7. Load-load-point displacement response of the cracking specimen under the loading described in Fig. 5 up to catastrophic failure at about $e/a = 0.0056$. Marked by Q is the displacement-controlled instability point.

length jumps suddenly from about 0.69 a to a and the equilibrium loading force per unit length drops to zero. Since we neglect the effect of inertia, this simulation cannot describe the instantaneous unstable crack growth in which the effect of inertia plays a significant role; the details of the simulation of dynamic crack growth can be found in Yang and Ravi-Chandar (1996) and Yang (1996).

The results described above indicate that *the complete process of generation of the fracture process zone and the growth of the crack tip are determined simply by solving the elastic boundary value problem*; this is the main result of this paper. With the prescription of the constitutive law for the cohesive zone, additional fracture criteria or parameters are not necessary for describing the initiation and continued growth of the crack. However, it must be noted that we have assumed that the cohesive zone is confined to a thin layer and that it forms straight ahead of the crack; for a bulk material, one would have to provide an evolution law for the transformation of the bulk material into the process zone and perhaps include other possible evolution of the crack tip processes such as thickening of the cohesive layer, crack kinking or branching. With this formulation, the idea of a stress intensity factor or energy release rate as a fracture characterizing parameter has been circumvented as well as the Dugdale-Barenblatt criterion, using the idea of vanishing of the singularity to determine the cohesive zone size; simply by limiting the maximum stress and the maximum displacement that the cohesive layer can sustain, the size of the cohesive zone and the growth of the crack are determined. While there might be merit in making comparisons to traditional fracture mechanics formulations—as we shall in later sections—we believe that the cohesive zone approach provides a more unified approach to considerations of fracture problems. Within the framework described above, we shall explore the cohesive zone model further in terms of its role in characterizing crack stability.

A number of simulations, with different initial crack lengths but with the same cohesive layer thickness, material properties, and initial damage in the cohesive zone size as in the previous simulation, were performed. In each of the simulations, the applied quasi-static displacement, $e(t)$, increased monotonically until the displacement-controlled instability of the specimen occurred. From these simulations we observe the following:

- The load vs the load-point displacement variation from these simulations are plotted in Fig. 8a; here one finds a locus for crack growth initiation in this specimen.
- The residual strength of a cracked structure is the maximum load or displacement that the structure is able to sustain without crack extension. The residual strength of the

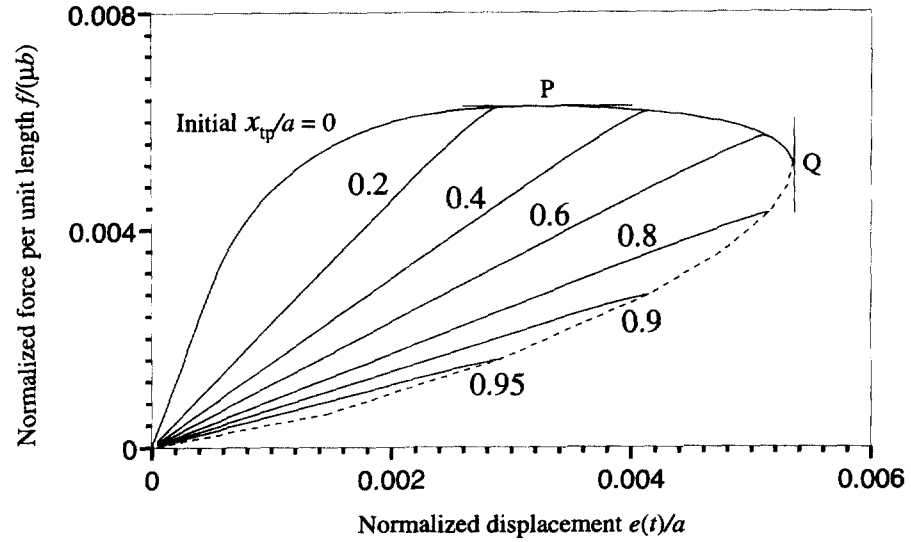

(a)

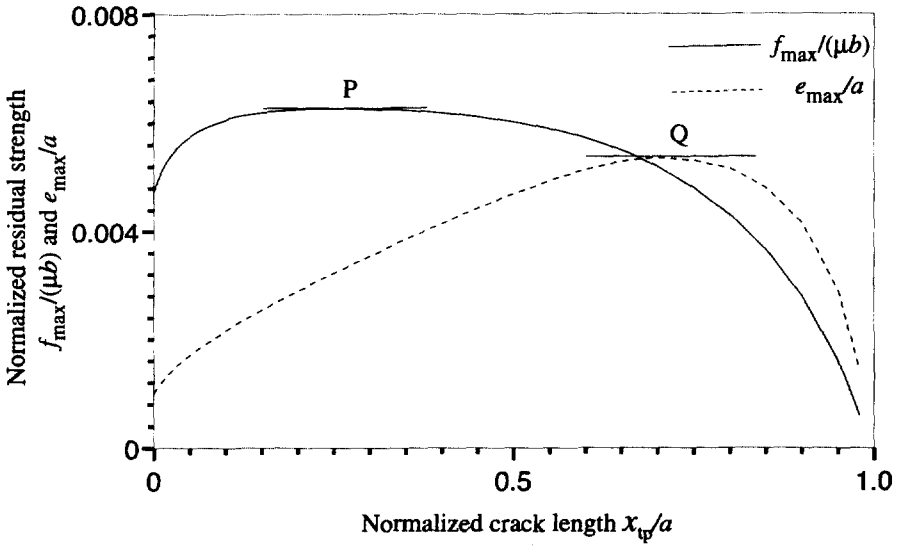

(b)

Fig. 8. Results of the simulations under the loading on the left boundary of the rectangular specimen shown in Fig. 1 : (a) f-e diagram in which the dashed line indicates the unstable fracture locus under the loading of displacement control; (b) residual strength vs crack length.

specimen expressed by both f_{max} and e_{max} is plotted vs normalized crack length x_{tp}/a in Fig. 8b, which reinterprets the fracture locus in Fig. 8a. Transition to unstable crack extension occurs at different points depending on whether boundary forces or displacements are controlled; the instability points under conditions of dead-load and displacement control are marked by P and Q respectively in Figs 8a and 8b. The instability points are determined to be correspondingly the maxima of the curves of the residual strength diagrams, which are marked by P and Q respectively in Fig. 8b.

- In the early stages of the loading, crack extension is stable with a steady-state cohesive process zone of size equal to 4.5 d; this is the equilibrium cohesive zone length and is characteristic of this material and loading configuration. This characteristic cohesive zone length is also the quasi-static limit resulting from a complete dynamic simulation of the fracture problem (see Yang and Ravi-Chandar, 1996).

- Stable crack growth is not observed at all if the initial crack length is over about 0.69 a, even under displacement-controlled loading. The process zone corresponding to the unstable initiation of crack growth is smaller than the equilibrium cohesive zone length indicating an incomplete development of the fracture process.

The model of a fracture process zone through a cohesive zone has enable a full-field simulation of crack growth without resorting to a singularity based fracture theory. Based on this model, we are able to examine many of the basic features of fracture mechanics. Discussions below will be focused on the role that the configuration plays cooperatively with cohesive layer material property in determining the stability of cracks, the validity of traditional one-parameter characterization of fracture through a critical value of the J-integral and COD for onset of the crack growth and the effects of variations in the cohesive zone properties on crack growth.

4.2. *Effect of loading configuration on crack growth*

The formulation of the crack growth problem through the cohesive zone model results in a description of the fracture problem as a structural stability problem in quite a similar way that the yielding concept leads to the plastic collapse formulation for strength of a structure. The concepts of brittle and ductile failure of a structure are reduced to a dimensional effect. In order to illustrate these ideas, a different loading configuration of the mode III problem is considered as shown in Fig. 9. The left and right boundaries are considered to be traction free; the top and bottom boundaries are displacement controlled as indicated in the figure. Due to the anti-plane symmetry of this loading configuration, only one half of the specimen needs to be considered. The material and geometric parameters are the same as in the earlier simulations. A number of simulations of different initial crack length were performed; the results of these simulations are shown in Fig. 10. With respect to the growth of the crack in this configuration we note the following:

- Figure 10a shows the variation of the load vs the load-point displacement at the top boundary; comparison to Fig. 8a for the load elongation curve indicates that this loading condition is much more stiff than the edge-loading configuration; the total stored elastic energy in the specimen is quite large compared to the fracture energy.
- Stable crack growth is not observed in this configuration; the crack growth initiation is unstable for all initial crack lengths under this loading configuration. In the numerical

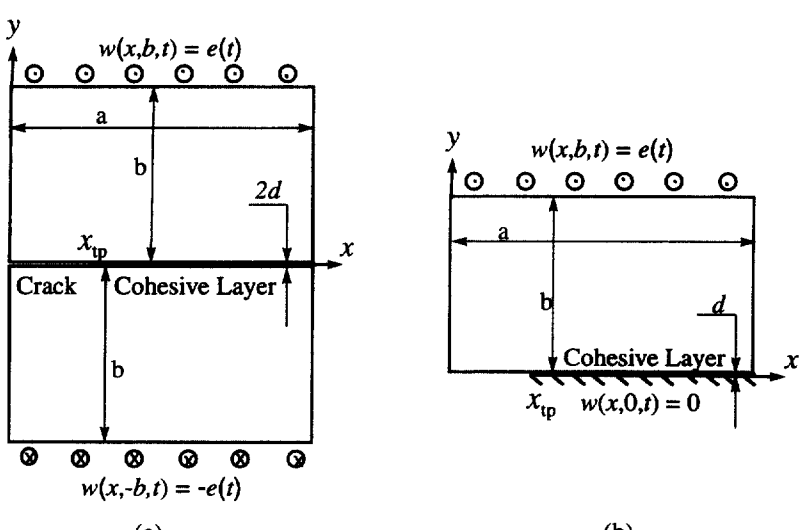

Fig. 9. (a) Geometry of the crack in a finite rectangular specimen with displacements prescribed on the top and bottom boundaries, under anti-plane shear with a cohesive layer material ahead of the crack tip, along the line $y = 0$; (b) geometry of the equivalent problem with zero displacement along the line $y = 0$.

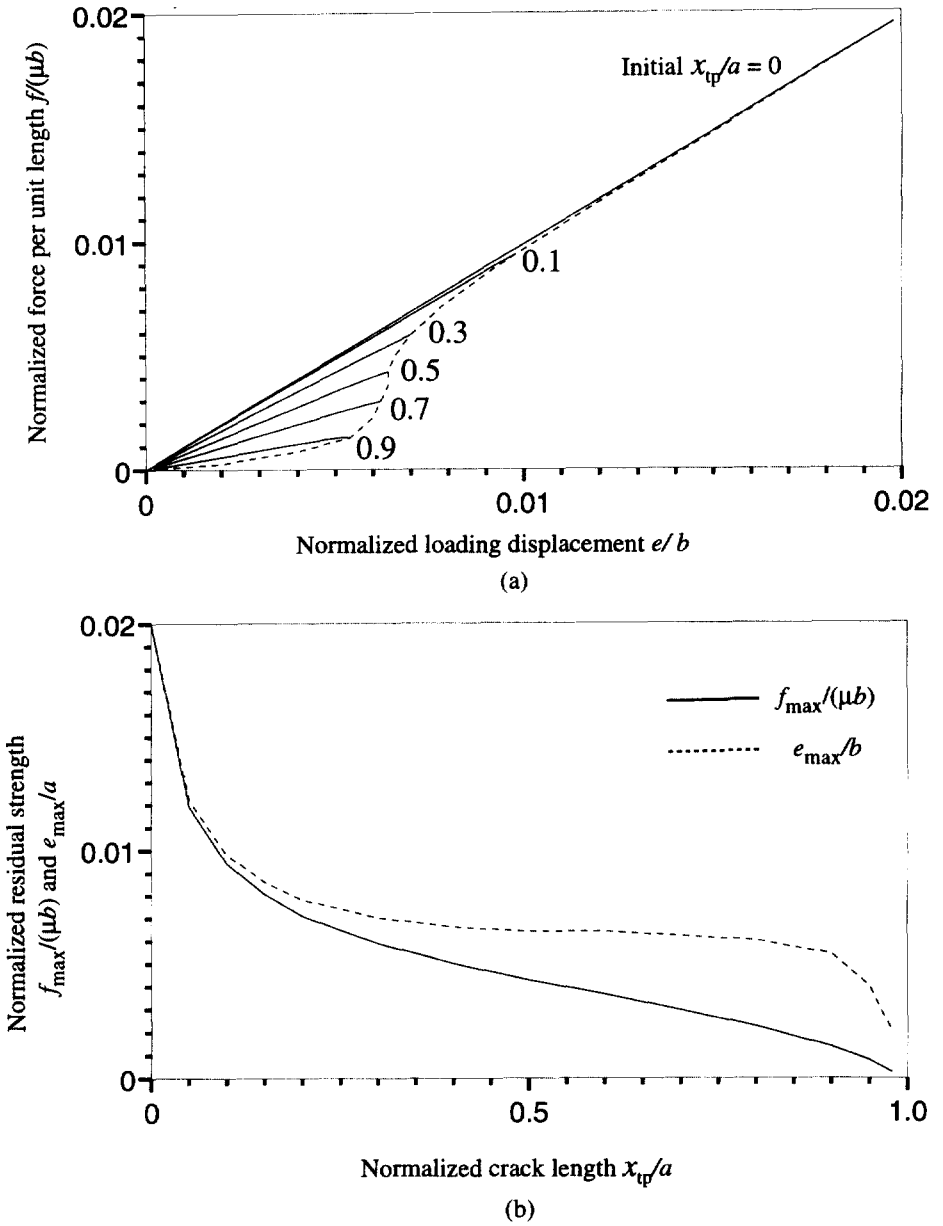

Fig. 10. Results of the simulations under the top-bottom loading condition of Fig. 9 : (a) f-e diagram in which the dashed line is the fracture locus which is unstable under the either dead-load or displacement control ; (b) residual strength vs crack length.

simulations, solutions are obtained by incrementing the global applied displacement and iterating for the displacement field ; beyond initiation, this iteration converges to a uniform displacement over the entire specimen, implying crack extension across the entire plate.

- The dependence of the residual strength of the specimen as a function of the crack length is shown in Fig. 10b ; the residual strength decreases monotonically again indicative of an unstable configuration. In fact, for crack lengths in the range of 0.25 a to 0.75 a, the residual strength variation with crack length indicates a square-root dependence suggestive of a brittle Griffith-type response of the cracked structure.
- This simulation includes an uncracked plate result as well ; this corresponds to two plates glued together, without a prenotch, but with a predamaged zone of size d. The entire unbroken segment of the cohesive layer is stressed to very nearly the peak stress of the layer, resulting in a large residual strength ; after a crack develops from this damage zone,

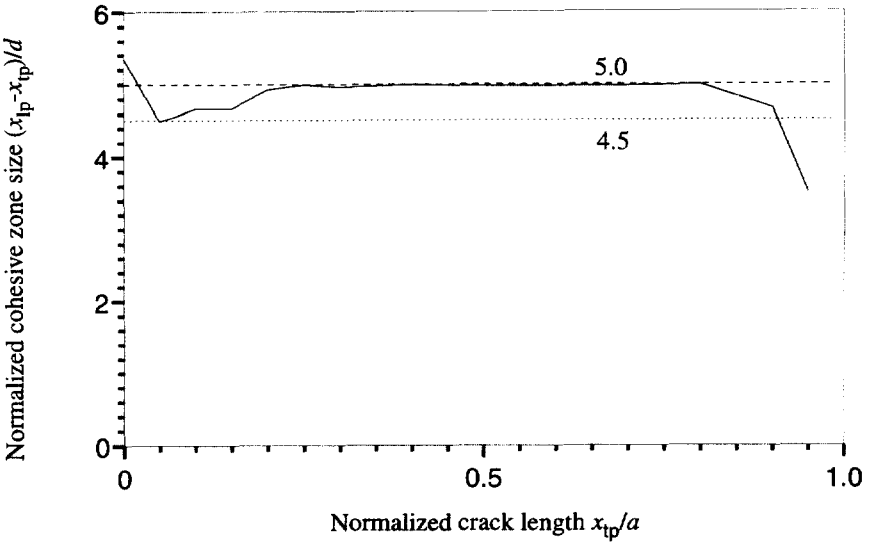

Fig. 11. Variation of the cohesive zone length at initiation of unstable crack growth in the top-loading configuration with the initial crack length. The dotted line indicates the cohesive zone size with which a crack advances stably in the edge loading configuration.

the residual strength drops significantly demonstrating the stress concentrating effect of the crack tip.

- The variation of the process zone size at transition to unstable growth as a function of the initial crack length in these simulations is shown in Fig. 11. For crack lengths in the range of 0.25 a to 0.8 a, the cohesive zone length is nearly constant at 5 d, somewhat larger than the equilibrium cohesive zone determined for the edge loading configuration. The implication is that the geometrical constraint of the present loading configuration plays a significant role in the development of the fracture process zone and in determining the size of the equilibrium cohesive zone; thus, while the dissipation in the fracture process zone is limited by the prescription of the cohesive layer constitutive model, the extent of the fracture process zone and the stability of its growth are determined by the geometrical constraint and loading configuration.

This result indicates that transferability of fracture parameters from one geometry to another has to be effected very carefully when one uses a single parameter fracture characterization, but with a full cohesive zone description of the fracture problem, this limitation does not arise.

4.3. *Examination of critical J-value and COD fracture criterion*

The modeling of crack initiation and growth through the description of a cohesive zone makes it possible to characterize fracture mechanics in terms of a simple elastic problem, with all the inelastic processes that lead to the development of the crack captured in the cohesive zone constitutive law. While the complete solution of the crack problem with this cohesive zone model obviates the need for a special fracture parameter, it also provides the possibility of evaluating the conditions under which a one-parameter characterization of the fracture that is typically used in fracture mechanics is adequate. We focus attention on two such parameters, the J-integral and the crack opening displacement (COD, $\delta = 2\, w(x, 0^+)$). For the cohesive zone model, the J-integral is given by

$$J = \int_{\delta_{lp}}^{\delta_{tp}} \tau_y(\delta) d\delta, \tag{24}$$

where, τ_y is the stress corresponding to the COD, δ, in the process zone, and δ_{lp} and δ_{tp} are respectively the displacements at the leading and trailing points of the process zone. The

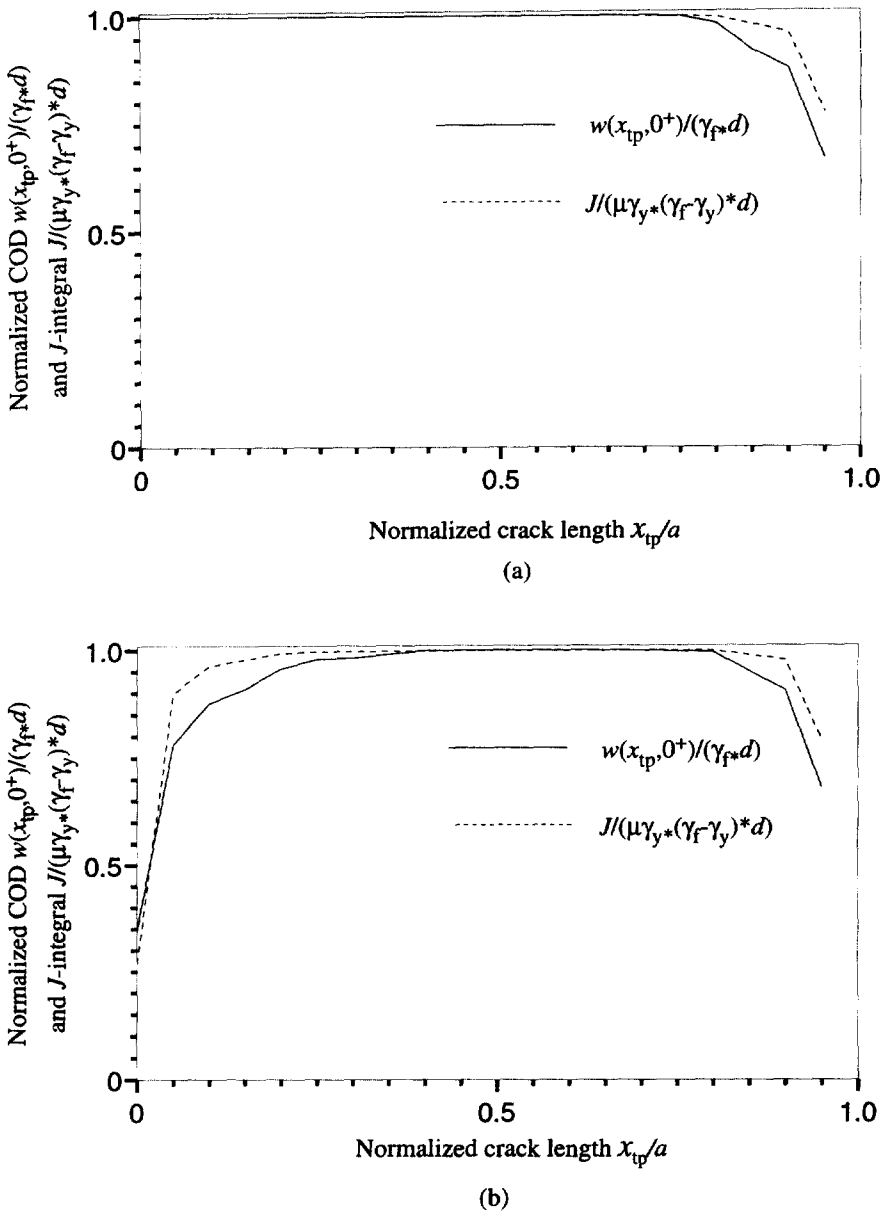

Fig. 12. Normalized critical COD and J-integral for the onset of either stable or unstable crack growth under the loading configurations: (a) edge loading shown in Fig. 1; (b) top-bottom loading shown in Fig. 9.

critical COD for onset of either stable or unstable crack growth is evaluated normally at the physical crack tip in this model and is equal to δ_{tp}.

In the simulation of the edge-loading problem, we observed stable crack growth with a fully developed process zone at small crack lengths and then the onset of unstable crack growth. In this case, the states of the process zone material are always on the damage locus indicated in Fig. 4, with $\delta_{tp} = \gamma_y \times 2d$ and $\delta_{tp} = \gamma_f \times 2d$. Thus, the J integral (24) for the onset and continued stable crack growth is simply given by the shaded area in Fig. 4 times the layer thickness $-J_s = \mu d\gamma_y(\gamma_f - \gamma_y)$; note that the elastic energy of layer deformation is not dissipated since we assume that there is a pre-existing cohesive layer. Thus we use the values of the COD and J-integral corresponding to stable crack growth as the normalizing parameters. Fig. 12 shows the variation of the normalized COD and J-integral as a function of the initial crack length for the edge-loading (Fig. 1) and top-loading (Fig. 9) specimen configurations. A number of observations are relevant to these results:

- For the edge-loaded configuration, during the stable cracking regime (initial crack length $< 0.69\ a$) single parameter characterization in terms of either the J-integral or the COD provides an adequate description of the fracture process; this is the region of self-similar crack extension with a fully developed process zone.
- For crack lengths larger than $0.69\ a$, the cohesive zone is not fully developed at the onset of structural instability implying that equilibrium solutions do not exist for these crack lengths for boundary displacements larger than the critical value; the values of the J-integral or the COD at the onset of unstable crack growth are clearly not a material property, but are dictated by a combination of material properties and structural constraint.
- For the top-loaded configuration, stable crack growth is not observed at all, and the values of the J-integral or the COD at the onset of unstable crack initiation varies significantly from the steady-state value J_s. For $0.25 < x_{tp}/a < 0.8$, the J-integral at the onset of unstable crack growth is almost constant and equal to J_s. For the small crack lengths, the global stress is a significant fraction of the peak stress in the layer, suggesting of a large-scale-yielding problem, but the resulting crack extension is unstable, suggesting "brittle" behavior!
- The obvious dependence of the COD and J-integral values on crack length and loading distribution indicates that these parameters are not true material properties and that the fracture theory founded on the asymptotic analysis of the local region at a crack tip can be only applied in restricted conditions. This, of course, is not a new result—a similar conclusion was reached by Ungsuwarungsri and Knauss (1987) and Smith (1995), based on their analysis of cohesive zone models. Also, in elastic plastic fracture analysis, geometrical constraint dependence of J-integral based fracture analysis has long been acknowledged.
- Two limitations, both relatable to a size effect, of the single parameter characterization are readily apparent: first, when either the crack length or the remaining unbroken ligament length is too small in comparison to a characteristic length scale—the fracture process zone size—a single parameter description becomes inadequate. From the simulations, we have a quantitative estimate of these sizes; it is surprising that the small crack or small ligament at the limit of one parameter characterization is in fact many times the equilibrium cohesive zone size. The second limitation arises from the geometric constraint provided by loading configuration that prevents the growth of the process zone to the steady-state length. In classical fracture mechanics, both these issues are addressed through modifications of the single parameter fracture characterization.

However, all these limitations are circumvented by using a complete simulation of the crack problem within the context of the cohesive zone model; the remaining problem then is to capture accurately the constitutive behavior of the cohesive zone! This problem typically needs to be addressed either through careful experimental characterization of the cohesive zone material or through a micromechanical model of the fracture process and is not considered here. In the following, we shall examine the influence of different types of cohesive zone material behavior on crack growth behavior which provides some insight into the problem of cohesive layer material property determination through experiments.

4.4. *Effect of cohesive zone material properties on crack growth*

In order to explore the influence of the cohesive zone properties on crack growth, simulations were performed using three different piece-wise linear constitutive laws as shown in Fig. 13. In the first material, there is a rapid initial drop in the cohesive layer stress and then a long, gradual decrease, indicative of brittle materials with a bridging zone such as ceramics and concrete. The second material simulates an elastic-plastic behavior of the layer for small strains and then a linear drop in the cohesive stress; note that the separation strain is one half of the first material. The third material is similar to the material used earlier in this paper, but with a smaller layer thickness which influences the stiffness of the layer. All three materials were selected to have the same energy dissipation in a stable fracture process. Here we consider only stable crack growth with a fully developed process

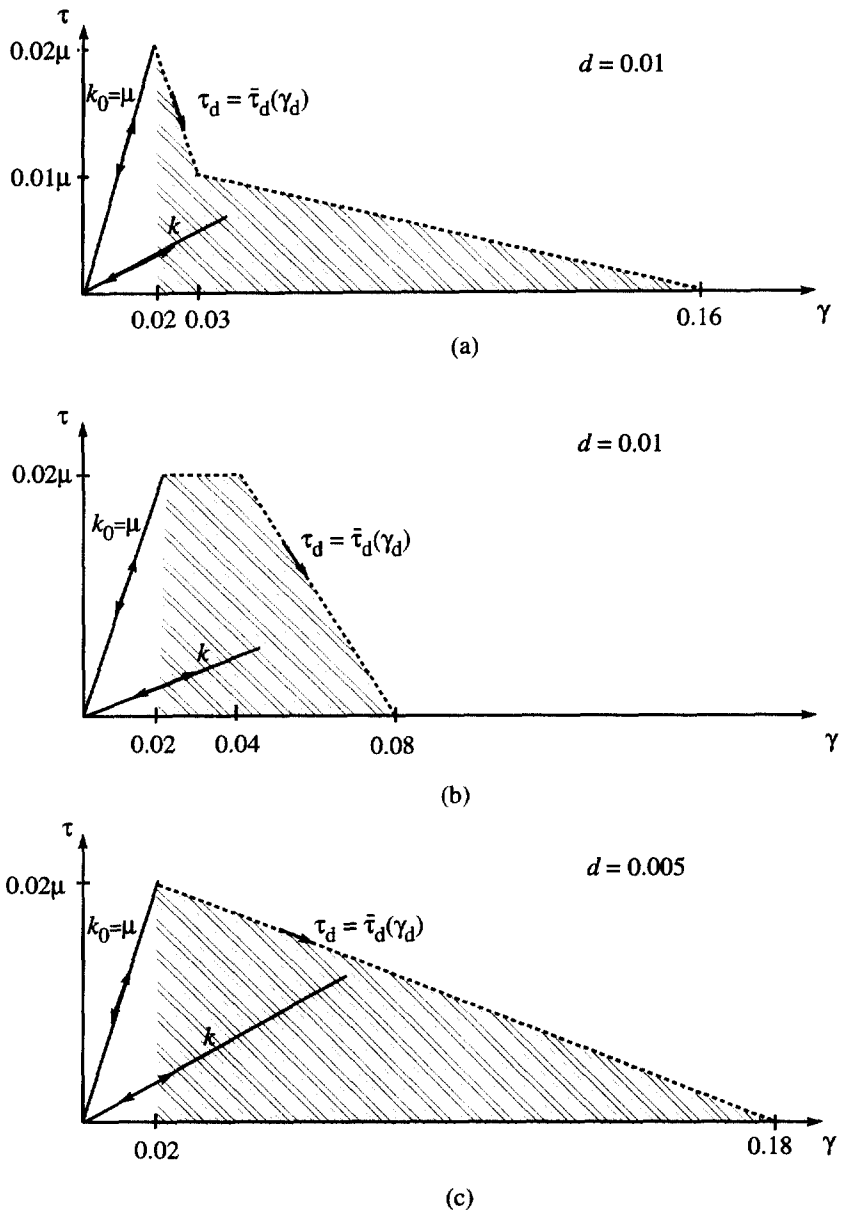

Fig. 13. Constitutive laws of the cohesive layer material used to examine the role of the process zone on crack growth behavior. The value of the shaded area times d in the diagrams is identical, which is the critical value of J-integral for stable crack growth.

zone, as provided by the loading configuration in Fig. 1. According to the definition in eqn (24), clearly the critical J-value for stable crack growth in the three different materials is the same; however, the corresponding critical CODs are obviously quite different. The main results of the simulations with these three cohesive zone materials are shown in Fig. 14. The load vs the load-point displacement variation is plotted in Fig. 14a, the variation of the normalized stress components σ_{zx} and σ_{zy} is shown in Fig. 14b and the crack opening profile is compared in Fig. 14c.

- In the results shown in Fig. 14a, one finds that all the load vs the load-point displacement curves are almost identical suggesting that *the global behavior of the cracking specimen is insensitive to the detailed shapes of the damage loci.*
- On the other hand, the local stress fields near the crack tips and the crack opening profiles in the process zones are very different, as illustrated in Fig. 14b and 14c, respectively.

- The size of the process zone is also quite different in the three different materials; the equilibrium cohesive zone lengths for the three materials are 11.8 d, 3.1 d and 4.5 d respectively, compared to 4.5 d for the material shown in Fig. 4.
- It is interesting to note that the profiles of the stress component σ_{zy} in the process zone are of similar shapes to the damaging loci shown in Fig. 13. Moreover, for material 2, the stress component σ_{zx} is larger than σ_{zy} suggesting that crack extension straight ahead may be unstable leading to kinking; of course, this possibility has been eliminated in the present simulation by imposing the anti-symmetry and the cohesive layer along this line of anti-symmetry.
- From the above simulations of different materials, we conclude that a *global measurement of the load and load-point displacements in a cracking specimen cannot be used to determine uniquely the detailed material properties in the fracture process zone; local measurements*

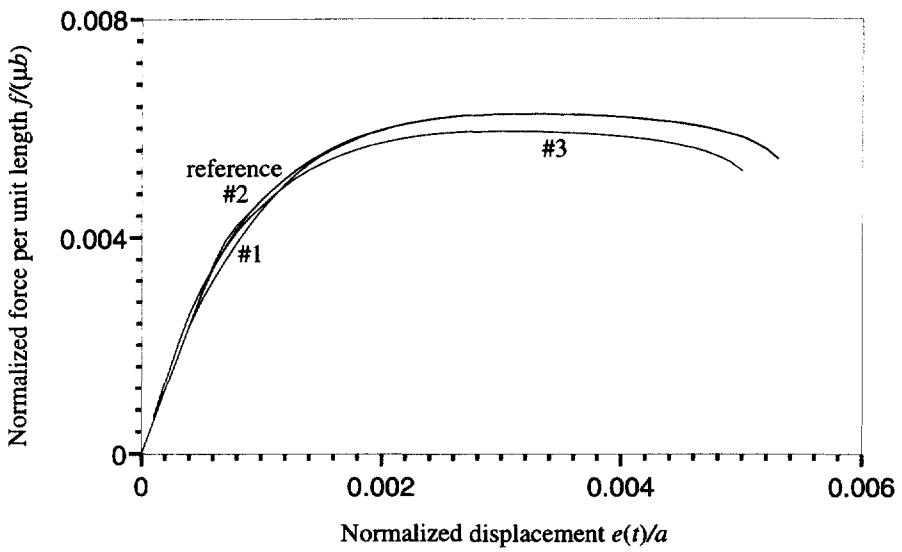

(a)

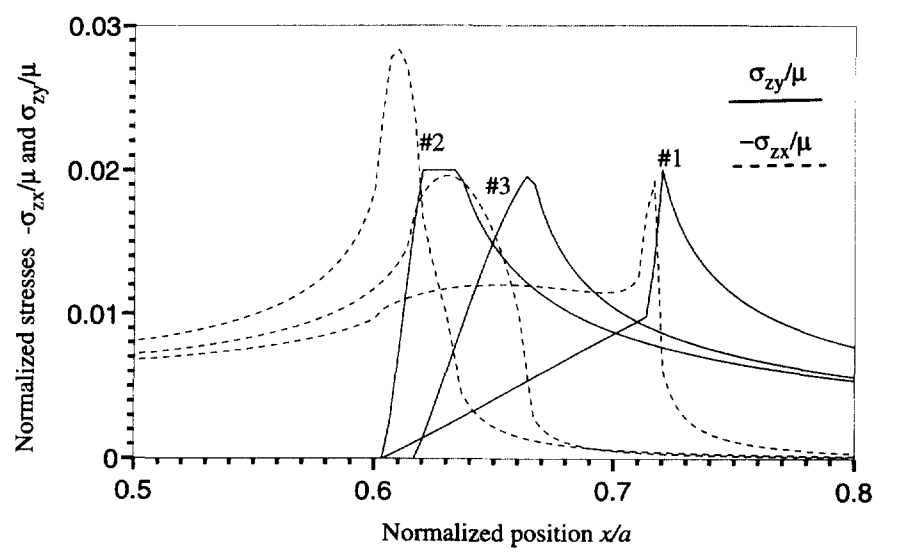

(b)

Fig. 14. Effect of the local constitutive properties in the process zone: (a) f–e diagram; (b) stress profiles along the upper layer boundary.

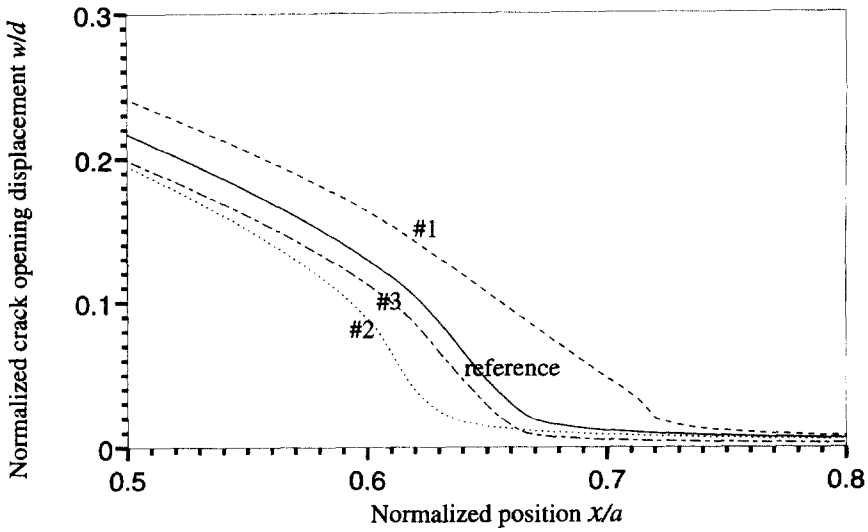

(c)

Fig. 14. (c) Crack opening profiles. The stress profiles in the reference simulation are almost the same as those in simulation #3 respectively.

are necessary for an accurate characterization of the cohesive zone properties. Recently, Alfredsson and Stigh (1997) have shown that by measuring the local displacement at the trailing edge of the cohesive zone in addition to the applied loading, the constitutive behavior of the cohesive layer material may be extracted exactly.

5. CONCLUSION

Modeling of crack initiation and crack growth with a fracture process zone represented by a cohesive zone was examined in this paper. The cohesive layer material was assumed to possess an elastic-softening type constitutive behavior. Implementing this model in a mode III setting, it was demonstrated that the associated boundary value problem is easily solved using finite difference methods; the initiation and growth of the fracture process zone as well as the initiation of crack growth are obtained naturally as a result of the simulation, without imposing additional fracture criteria. The results are discussed with respect to considerations of stability of crack growth, traditional critical fracture parameters such as the COD and J-integral and the influence of the assumed constitutive model for the cohesive layer. It is demonstrated that single parameter fracture characterization does not always hold in different geometric and loading configurations, but that the cohesive zone model provides a unified way of examining the problem. Also, it is found that differences in the constitutive behavior of the layer material may not manifest themselves in the global load vs the load-point displacement behavior of the specimen, but will be apparent in the local parameters, pointing to the need for local measurements when characterizing the material model. In summary, if an accurate description of the cohesive zone constitutive law is obtained through experiments with local measurements, the complete fracture problem can be addressed using the approach described here, without resorting to additional fracture criteria or parameters.

Acknowledgement—The research support of the Air Force Office of Scientific Research during the course of this work is gratefully acknowledged.

REFERENCES

Alfredsson, K. S. and Stigh, U. (1997) A method to determine constitutive properties of thin interface layers loaded in shear. *Advances in Fracture Research* (ed. B. L. Karihaloo *et al.*), Pergamon, New York, pp. 2667–2674.

Andersson, H. and Bergkvist, H. (1970) Analysis of a non-linear crack model. *Journal of the Mechanics and Physics of Solids* **18,** 1–28.

Barenblatt, G. I. (1962) The mathematical theory of equilibrium cracks in brittle fracture. *Advances in Applied Mechanics* (ed. H. L. Dryden and T. von Karman), Academic Press, New York, pp. 55–129.

Bennison, S. J. and Lawn, B. R. (1989) Role of interfacial grain-bridging sliding friction in the crack-resistance and strength properties of nontransforming ceramics. *Acta Metallurgica et Materialia* **37,** 2659–2671.

Bosco, C. and Carpinteri, A. (1995) Discontinuous constitutive response of brittle matrix fibrous composites. *Journal of the Mechanics and Physics of Solids* **43,** 261–274.

Carpinteri, A. (1994) Cracking of strain-softening materials. In *Static and Dynamic Fracture Mechanics* (ed. M. H. Aliabadi, C. A. Brebbia and V. Z. Parton), Computational Mechanics Publications Inc.

Cox, B. N. and Marshall, D. B. (1994) Concepts for bridged cracks in fracture and fatigue. *Acta Metallurgica et Materialia* **42,** 341–363.

Dugdale, D. S. (1960) Yielding of steel sheets containing slits. *Journal of the Mechanics and Physics of Solids* **8,** 100–104.

Hay, J. C. (1995) High temperature characterization of microstructural mechanisms affecting grain bridging in monolithic structural ceramics, Ph.D. Dissertation, University of Houston.

Hillerborg, A., Modéer, M. and Petersson, P. E. (1976) Analysis of crack formation and crack growth in concrete by means of fracture mechanics and finite elements. *Cement and Concrete Research* **6,** 773–782.

Jagota, A. and Bennison, S. J. (1995) Element breaking rules in computational models for brittle fracture. *Modelling and Simulation in Materials Science and Engineering* **3,** 485–501.

Knauss, W. G. (1974) On the steady propagation of a crack in a viscoelastic sheet: Experiment and analysis. *Deformation and Fracture of High Polymers* (ed. H. H. Kausch *et al.*), Plenum Press, New York, 501–540.

Knauss, W. G. (1993) Time dependent fracture and cohesive zones. *Transactions of the ASME, Journal of Engineering Materials and Technology* **115,** 262–267.

Kendall, K., Clegg, W. J. and Gregory, R. D. (1991) Growth of tied cracks: A model for polymer crazing. *Journal of Materials Science Letters* **10,** 671–674.

Marshall, D. B., Cox, B. N. and Evans, A. G. (1985) The mechanics of matrix cracking in brittle-matrix fiber composites. *Acta Metallurgica et Materialia* **33,** 2013–2021.

Ortiz, M. (1996) Computational micromechanics. *Computational Mechanics* **18,** 321–338.

Schapery, R. A. (1975) A theory of crack initiation and growth in viscoelastic media. *International Journal of Fracture* **11,** 141–159, 369–388, 549–562.

Smith, E. (1974) The structure in the vicinity of a crack tip: A general theory based on the cohesive zone model. *Engineering Fracture Mechanics* **6,** 213–222.

Smith, E. (1995) The non-uniqueness of the maximum load J-value with a cohesive zone model of an elastic/softening solid. *Engineering Fracture Mechanics* **52**(4), 765–771.

Ungsuwarungsri, T. and Knauss, W. G. (1987) The role of damage-softened material behavior in the fracture of composites and adhesives. *International Journal of Fracture* **35,** 221–241.

Xu, X.-P. and Needleman, A. (1994) Numerical simulations of fast crack growth in brittle solids. *Journal of the Mechancis and Physics of Solids* **42,** 1397–1434.

Yang, B. and Ravi-Chandar, K. (1996) On the role of the process zone in dynamic fracture. *Journal of the Mechanics and Physics of Solids* **44,** 1955–1976.

Yang, B. (1996) Numerical simulations of crack growth with a fracture process zone, M.S. Thesis, University of Houston.